Journal of Korean Association of Crystal Growth
Vol. 7, No. 2 (1997) 197-206

# 6H-SiC epitaxial growth and crystal structure analysis

Kook-Sang Park and Ky-Am Lee
*Department of Physics, Dankook University, Cheonan 330-714, Korea*

# 6H-SiC 에피층 성장과 결정구조 해석

박국상, 이기암
단국대학교 물리학과, 천안, 330-714

Abstract A SiC epilayer on the 6H-SiC crystal substrate was grown by chemical vapor deposition (CVD). The crystal structure of the SiC epilayer was investigated by using the X-ray diffraction patterns and the Raman scattering spectroscopy. The SiC epilayer on the 6H-SiC substrate was grown to be homoepilayer by CVD. In order to distinguish a certain SiC polytype mixed in the SiC crystal grown by the modified Lely method, we have calculated the X-ray diffraction intensities and Bragg angles of the typical SiC crystal powders. By comparing the measured X-ray diffraction pattern with the calculated ones, it was identified that the SiC crystal grown by the modified Lely method was the 6H-SiC crystal mixed some 15R-SiC.

요 약 6H-SiC 위에 SiC 에피층이 화학 기상 증착(CVD)에 의하여 성장되었다. 성장된 SiC 에피층의 결정구조는 X-선 회절과 Raman 분광을 사용하여 조사되었으며, 이 에피층은 6H-SiC로서 성장되었음을 확인하였다. 수정된 Lely법으로 성장된 한 SiC 결정 분말의 결정구조를 확인하기 위하여 전형적인 SiC polytype들의 X-선 회절상을 계산하였으며, 측정된 X-선 회절상과 비교하여 이 SiC 결정에는 15R-SiC가 약간 혼재되어 있음을 확인하였다.

---

1) The CVD growth systems of the SiC epilayer and the modified Lely system were set up at Matsunami Laboratory in Kyoto University.

## 1. Introduction

In a crystallographic point of view, SiC is a famous material to show the various polytypism (more than 200 kinds). SiC polytypism is a phenomenon of making different crystal structures with same chemical composition. The energy gap of SiC varies from 2.4 eV to 3.3 eV depending on the SiC polytypes of many crystalline forms. SiC has the electrical property depending on the specific polytype. Accordingly, it is important to control the polytypes for the application to semiconductor devices. However, SiC growth can inevitably bring about the problem of the contained polytypes and the unwanted impurities in growing of the epilayer of SiC. Because the stacking sequence of Si-C pairs on the sub-layer is influenced by the surface potential, the impurities and the defects. The polytype inheritance can occur during the crystal growth. Figure 1 shows the occurrence of SiC polytypes with increasing the growth temperature [1]. The SiC crystal structures can vary, under differing growth conditions involving temperature, pressure, growth rate. Accordingly, whenever the crystal structures are investigated by X-ray diffraction, the peak intensities can be either increased or decreased, and either appeared or disappeared, and the Bragg angles can be shifted. The origin of polytype formation has remained as an interesting and open question in spite of the efforts by many investigators [1].

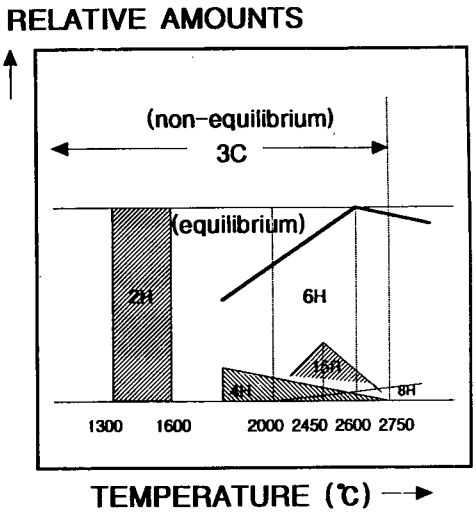


Fig. 1. Occurrence of SiC polytypes with increasing the temperature [1].

In this study, a SiC epilayer on the 6H-SiC crystal was grown by chemical vapor deposition (CVD). The structure of the epilayer are identified by using the X-ray diffraction patterns and the Raman scattering spectroscopy [2-4]. The X-ray diffraction patterns of several typical SiC polytypes were simulated to find out which SiC polytypes were contained in a certain SiC crystal powder. The crystal structure of a crystal powder was identified by comparing the measured the X-ray diffraction patterns with the calculated ones.

## 2. Experiments

### *2.1. SiC epitaxial growth*

A SiC epilayer sample was grown by CVD along the c-axis of the 6H-SiC substrate [5]. Figure 2 shows the schematic diagram for

the CVD growth apparatus[1]. The CVD growth was carried out at 760 torr. $SiH_4$ (1 %) and $C_3H_8$ (1%) diluted with $H_2$ gas were used as the source gases. The $H_2$ gas, which was the carrier gas durig CVD, was purified through an Ag-Pd purifier. The susceptor in the reaction tube was heated up by RF induction with a frequency of 400 kHz and a power of 15 kW. In order to create a uniform thickness in the epilayers, the susceptor was inclined at an angle of 10° toward the upper gas flow stream. The gas flow and temperature program during the CVD growth is shown in Fig. 3. Prior to the CVD growth, the susceptor was baked out at 1500℃ for 12 minutes in $H_2$ ambience at 760 torr. The SiC substrates were etched by HCl (100 %) gas at 1300℃ for 10 minutes to clean the surfaces chemically just before the start of the CVD growth. After the etching was stopped by shutting off HCl flow, the temperature was decreased down to 800 ℃ while the $H_2$ flow rate was increased up to 3.0 slm. To flush residual HCl from the reaction tube, $H_2$ gas was continued to flow for 5 minutes at 800℃. After the flush of HCl, the substrate temperature was increased again up to a desirable growth temperature of 1500℃. The flow rate of $C_3H_8$ gas was varied in the range of 0.20 sccm by keeping the flow rate of $SiH_4$ fixed at 0.30 sccm, and the growth temperature was 1500℃. Off-orientation of the samples was 3.5° toward [11$\bar{2}$0]. A growth rate of about 2.4 $\mu$m/h was obtained under these growth conditions.

In order to study the SiC crystal structure, a 6H-SiC crystal is prepared, which is grown by the modified Lely method[1].

### 2.2. *X-ray diffraction pattern*

The X-ray diffraction patterns were mea-

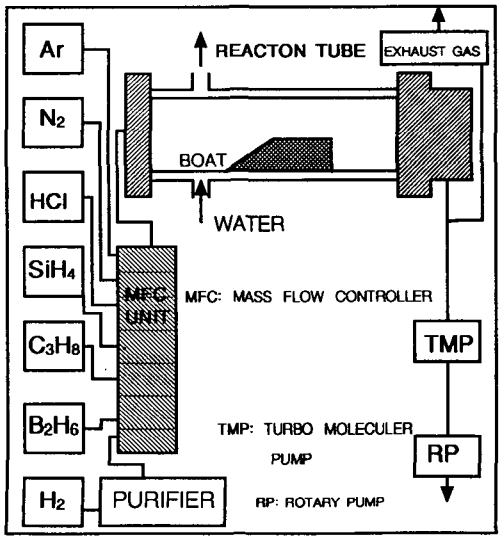


Fig. 2. A schematic diagram of CVD growth system[1].

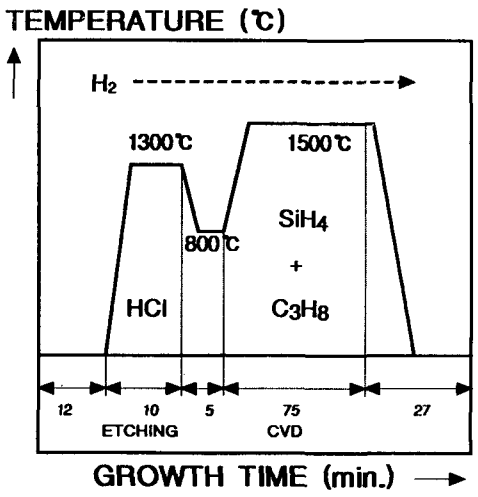


Fig. 3. The gas flow and temperature program for the CVD growth.

sured by using the X-ray diffractometer with the filtered Cu-k$\alpha$($\lambda$=1.5418Å) radiation. The epilayer on 6H-SiC substrate is rotated constantly along the c-axis during the measurement of the X-ray diffraction. Figure 4 shows the X-ray diffraction pattern from the (0001) plane of a 6H-SiC epilayer grown on the 6H-SiC crystal.

To identify the crystal structure of the 6H-SiC crystal substrate, it is rotated constantly along the c-axis during the measurement of the X-ray diffraction [6]. Figure 5 shows the X-ray peaks diffracted by the Cu-k$\alpha$ radiation from the (0001) plane of a 6H-SiC crystal substrate rotated around c-axis.

As for the SiC crystal powder, the diffracted intensities are measured over $2\theta$ angles from 20° to 90° with step interval of 0.02° and the scanning speed of 0.04° in $2\theta$ per second. The X-ray diffraction pattern of the 6H-SiC crystal powder is shown in Fig. 6. The X-ray peak intensities and Bragg angles are listed in Table 1.

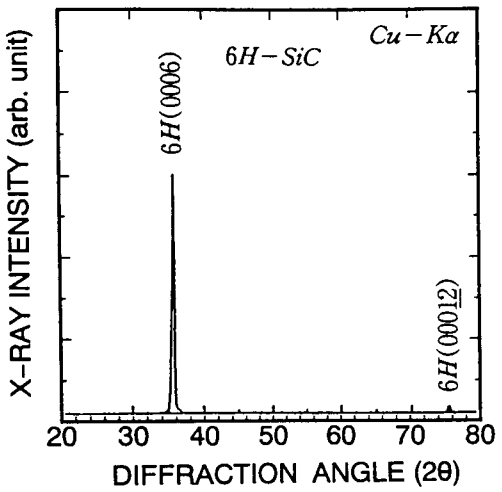


Fig. 4. The measured X-ray diffraction pattern of a 6H-SiC epilayer ([0001] direction).

### 2.3. *Raman spectra*

Raman spectra of the 6H-SiCs were

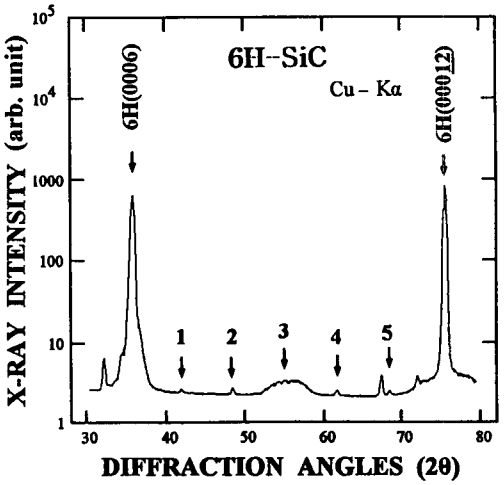


Fig. 5. The measured X-ray diffraction pattern of a 6H-SiC crystal substrate ([0001] direction) rotated around the c-axis.

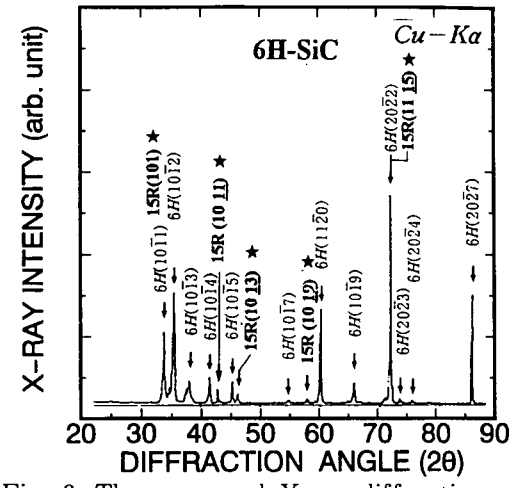


Fig. 6. The measured X-ray diffraction pattern of a 6H-SiC crystal powder.

measured in back scattering geometry by using the wavelength of 325 nm of He-Cd laser at room temperature. The incident light for the excitation was normal to the SiC epilayer surfaces. The scattered light was detected by using the model of RAMANOR U-1000 (JOBIN YVON Co.). The Raman spectrum of a SiC epilayer is shown in Fig. 7(a). The Raman peaks were observed at 967 $cm^{-1}$ for the longitudinal optic (LO) region, and at 768 $cm^{-1}$, 790 $cm^{-1}$, 799 $cm^{-1}$ for the transverse optic (TO) region. Figure 7(b) shows the Raman spectrum of a 6H-SiC crystal powder. The Raman peaks were observed at 970 $cm^{-1}$ for the longitudinal optic (LO) region, and at 766 $cm^{-1}$, 788 $cm^{-1}$, 797 $cm^{-1}$ for the transverse optic (TO) region.

Table 1
The measured intensities and Bragg angles of a 6H-SiC crystal powder diffracted by the X-ray with the filtered Cu-K$\alpha$

| Polytype(Planes) | | Diffraction angles($2\theta$) | Relative intensity |
|---|---|---|---|
| 6H($10\bar{1}1$) | | 34.000 | 33.9 |
| 6H($10\bar{1}2$) | 15R(005) | 35.560 | 53.4 |
| 6H($10\bar{1}3$) | | 38.160 | 10.6 |
| 6H($10\bar{1}4$) | | 41.520 | 11.1 |
| | 15R($10\underline{1}1$) | 42.780 | 6.7 |
| 6H($10\bar{1}5$) | | 45.330 | 10.7 |
| | 15R($10\underline{1}3$) | 46.295 | 4.8 |
| 6H($10\bar{1}7$) | | 54.675 | 1.4 |
| | 15R($10\underline{1}9$) | 57.720 | 2.0 |
| 6H($10\bar{1}8$) | | 59.865 | 55.5 |
| 6H($11\bar{2}0$) | 15R($10\underline{1}1$) | 60.030 | 45.6 |
| 6H($10\bar{1}9$) | | 65.790 | 9.6 |
| 6H($20\bar{2}1$) | | 70.810 | 2.3 |
| | 15R(201) | 71.665 | 100.0 |
| 6H($20\bar{2}2$) | | 71.835 | 53.4 |
| 6H($20\bar{2}3$) | | 73.360 | 1.9 |
| 6H($20\bar{2}4$) | | 75.525 | 1.0 |
| 6H($20\bar{2}5$) | | 78.265 | 0.3 |
| 6H($20\bar{2}7$) | | 85.470 | 53.4 |

## 3. Simulation of X-ray diffraction patterns

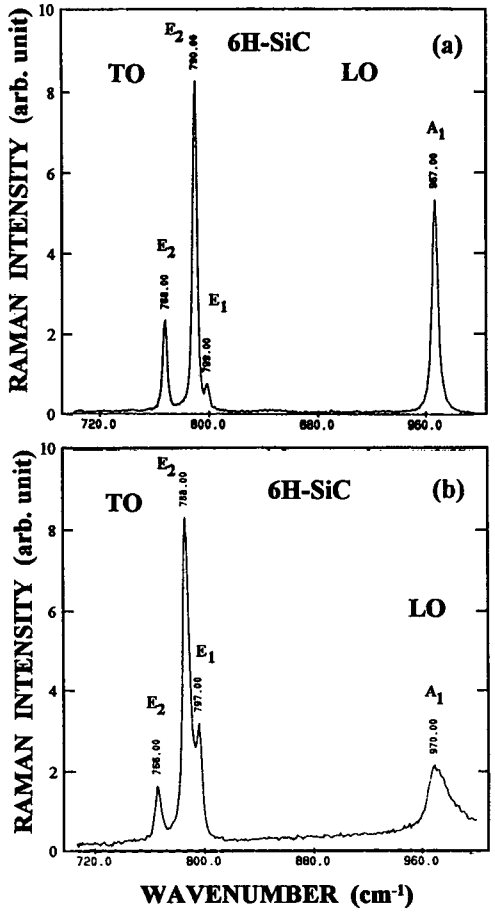


Fig. 7. Raman spectra of the optical pho nons; (a) a 6H-SiC epilayer and (b) a 6H SiC crystal powder.

For the X-ray diffractometer, there are five factors affecting the relative intensities of the diffraction lines on the X-ray powder diffraction : structure factor, $|F_{hkl}|$ multiplicity factor $p_{hkl}$, Lorentz-polarization factor $(1-\cos^2 2\theta)/(\sin^2\theta\cos\theta)$, absorption factor $A(\theta)$, and temperature factor $e^{-2M}$. The diffraction intensity $I_{hkl}$ for the X-ray diffractometer is calculated by

$$I_{hkl}=|F_{hkl}|^2 p_{hkl}\left[\frac{1-\cos^2 2\theta}{\sin^2\theta\cos\theta}\right]A(\theta)e^{-2M} \quad (1)$$

The structure factor $F_{hkl}$ for the (hkl) reflection is given by

$$F_{hkl}=\sum_n f_n \exp[2\pi i(hx_n+ky_n+lz_n)] \quad (2)$$

where the summation extends over all the n atoms of a unit cell, $f_n$ is atomic scattering factor, and the quantity M depends on both the amplitude of thermal vibration of atoms and the diffraction angle $2\theta$ [7]. The Lorentzian distribution of the diffraction intensities can be given by

$$I(2\theta)=\sum_p \frac{I_p(2\theta)r}{(2\theta-2\theta_p)^2+r^2/4} \quad (3)$$

where p is the number of diffraction line, $r$ the line width of the diffraction lines, and $I_p$ and $\theta_p$ are the intensity and Bragg angle of the p-th order diffraction, respectively. Besides, the Bragg law is

$$\lambda=2d_{hkl}\sin\theta, \quad (4)$$

for a incident wavelength $\lambda$, where $d_{hkl}$ is the spacing distance between adjacent planes in the set (hkl). In the cubic crystal, the distance $d_{hkl}$ is given by

$$\frac{1}{d_{hkl}}=\frac{h^2+k^2+l^2}{a^2} \quad (5)$$

where $a$ is a lattice constant of a unit cell. If the crystal has the hexagonal structure with the lattice constants of $a_o$ and $c_o$, the distance $d_{hkl}$ is given by

$$\frac{1}{d_{hkl}}=\frac{4}{3}\left(\frac{h^2+hk+k^2}{a_o^2}\right)+\frac{l^2}{c_o} \quad (6)$$

Figure 8 shows the stacking sequence of the SiC polytypes and the occupation sites of Si-C pairs along the c-axis ([0001] direction) of SiC in a close-packing system. Si-C pairs with short bonding length 1.89Å in each planes can occupy one of three sites denoted by A, B and C. 3C-SiC, zinc blende

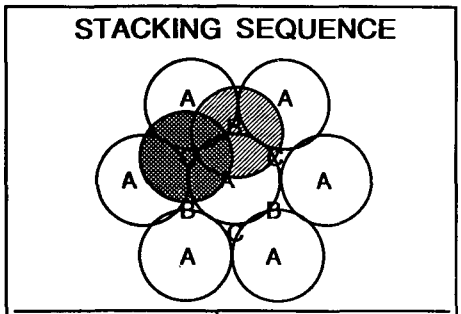


| POLYTYPES | STACKING |
|---|---|
| 2H-SiC | ABABAB ..... |
| 3C-SiC | ABCABC ..... |
| 4H-SiC | ABCBABCB ..... |
| 6H-SiC | ABCACB ..... |
| 15R-SiC | ABCACBCABACABCB |

Fig. 8. The stacking sequence of the SiC polytypes and the occupation sites of Si-C pairs.

structure, has 3 pairs of Si-C in an unit cell with the lattice parameter of 4.34Å and the stacking sequence of ABCABC··· as shown in Fig. 8. 4H-SiC and 6H-SiC, hexagonal structures, have 4 and 6 pairs of Si-C in an unit cell, respectively. The lattice parameters are $a_o$=3.09Å and $c_o$=10.08Å for the 4H-SiC and $a_o$=3.09Å and $c_o$=15.12Å for the 6H-SiC, respectively. 15R-SiC has 15 pairs of Si-C pair in a unit cell. The lattice parameters are $a_o$=3.09Å and $c_o$=37.30Å [1].

In order to analyze the measured X-ray diffraction lines, the X-ray diffraction patterns of the 3C-, the 4H-, the 6H- and the 15R-SiC crystals are calculated. The temperature factor is neglected, and the relative intensities and the Bragg angles diffracted from each plane can be calculated by using Eqs. of (1), (4), and (5). Figure 9 shows the calculated X-ray diffraction patterns of the SiC-polytype crystal powders diffracted by the Cu-k$\alpha$ radiation. It is assumed that the diffraction intensity of each line is distributed as a Lorentzian form with each line width of 0.2° in diffraction angle $2\theta$ [8].

Even if a certain SiC crystal seems to be perfect, it would not be completely excluded a possibility to exist another polytypes in a certain SiC. Then, the analysis of the varied X-ray diffraction intensities and Bragg angles can be used as a considerable means of the polytypes classification. Nevertheless, it should be considered that the precision of the other polytype content would be limited by the X-ray

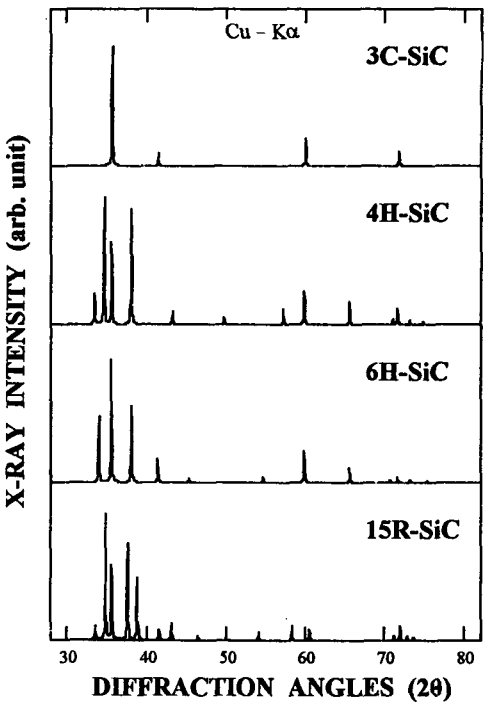


Fig. 9. The calculated X-ray diffraction powder patterns of the SiC polytypes.

resolution. The variation of the diffraction pattern was calculated by assuming that other polytypes were mixed in a certain SiC crystal. Figure 10 shows the calculated X-ray diffraction patterns with varying the composition w of the crystal $3C_{1-w}4H_w$ 6H. The peaks of the 4H-SiC polytypes would be obviously varied in the range of the diffraction angles from 30° to 50°. As the mixed rate w in 6H-SiC are increased, the intensities of the peak 1 {4H(10$\bar{1}$1)}and the peak 5 {4H(10$\bar{1}$3)}+6H(10$\bar{1}$5)} are relatively increased as shown in Fig. 10. The intensity of the peak 4 {4H(10$\bar{1}$3)+3C (200)+6H(10$\bar{1}$4)} can be relatively compared with those of the peaks of 5 and 6. The peaks of 2, 3 and 6 are diffracted

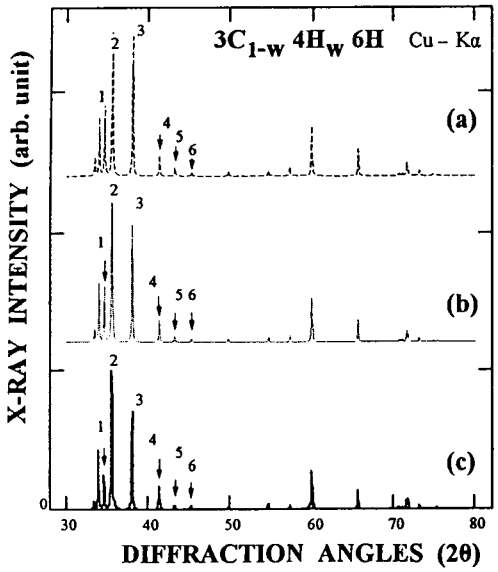


Fig. 10. The calculated X-ray diffraction spectra with varying the composition w of the crystal $3C_{1-w}4H_w6H$;(a) w=0.3, (b) w =0.5, and (c) w=0.7.

from the planes of {3C(111)+6H(10$\bar{1}$2)}, {3C(200)+6H(10$\bar{1}$4)} and 6H(10$\bar{1}$5), respectively. When the difference of the peak intensities is not clear, the effective means to confirm the existence of the polytypes is precisely to read the values of Bragg angles. However, it is difficult to distinguish the peak intensities and the Bragg angles of the 3C-SiC from those of the 6H-SiC lines, because the 3C-SiC peaks are almost overlap over the 6H-SiC peaks as shown in Fig. 9.

In order to identify the existence of the 15R-SiC polytype in the 6H-SiC crystal, we also calculated the diffraction intensities and the Bragg angles of the $15R_{1-x}$ $6H_x$ by assuming that the 15R-polytype was distributed to be the mixed rate (1−x) in a 6H-SiC crystal. Figure 11 shows the X-ray diffraction pattern of the $15R_{1-x}$ $6H_x$ when the ratio x is 0.1.

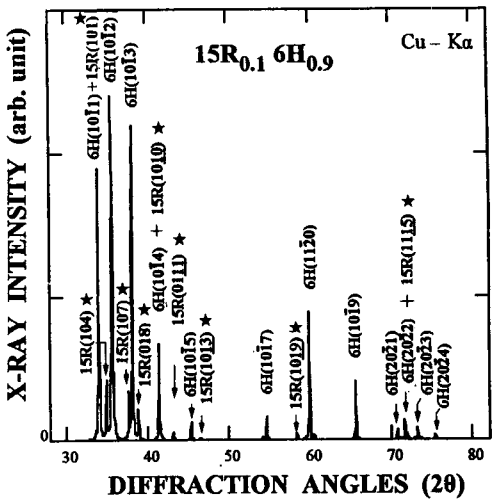


Fig. 11. The calculated X-ray diffraction spectrum of the $15R_{0.1}6H_{0.9}$ crystal powder.

## 4. Results and discussion

The X-ray diffraction pattern of the SiC crystal powder, as shown in Fig. 6, clearly indicates a SiC crystal grown as 6H-SiC polytype. The 6H-SiC peaks appeared together with those of another polytypes. The diffraction intensities and Bragg angles of the measured 6H-SiC diffraction lines were almost coincided with those of the calculated 6H-SiC's as shown in Fig. 11, but it is shown a few peaks which can not appear in the 6H-SiC diffraction pattern. The other peaks except the 6H-SiC's can not be diffracted from either the planes of the 3C-SiC or the 4H-SiC. The peaks marked with

"star" in Fig. 11 can be diffracted from 15R (104), 15R (107), 15R (108), 15R (01$\underline{11}$), 15R (10$\underline{13}$), and 15R (10$\underline{19}$) planes of the 15R-SiC, respectively. Simultaneously, the other peaks of 15R (101), 15R (10$\underline{10}$) and 15R (11$\underline{15}$) can nearly overlap those of 6H (10$\bar{1}$1), 6H (10$\bar{1}$4) 6H (20$\bar{2}$2), respectively. It was identified by the X-ray powder diffraction that the SiC crystal was grown as a 6H-SiC which contained some 15R-SiC polytype. The rate of the 15R-SiC polytype mixed in the 6H-SiC crystal is difficult to estimate acculately.

However, the X-ray powder method is enervated when the crystal structure of the single crystal or the epitaxial layer is analyzed by the X-ray diffraction, because the grown samples must be well kept so as not to break during the measurement. It has well known that the 4H-SiC and the 6H-SiC single crystals of the hexagonal type can be confirmed by the X-ray diffraction patterns from the (0001) plane of each sample. Then, they are rotated constantly along the c-axis during the measurement of the X-ray diffraction. According to the extinction rule of the space group ($P6_3mc$) for the hexagonal structure, only the (000$\ell$) peaks appear, where $\ell$ is 2n (n:positive integer). In Fig. 5, there are two main peaks of 6H (0006) and 6H(00012) for the 6H-SiC structure in the same [0001] direction. In the 6H-SiC crystal, five weak sub-peaks can be observed between two main peaks. These peaks result from X-ray double reflection, since these peaks were appeared by a small precession of the [0001] direction for the X-ray incident angle. The subpeaks were about one or two hundredth of the main peak intensity. The 6H-SiC crystal substrate was identified by the five weak sub-peaks of the diffraction pattern.

As for the SiC epilayer grown by CVD, the crystal structure was investigated by using the X-ray diffraction pattern as shown in Fig. 4. Even though these peaks were diffracted from the planes of the 6H-SiC, it may not be completely excluded the possibility that such peaks can be diffracted from several planes of the 3C-SiC. The diffraction lines of the 3C-SiC polytype are difficult to be distinguished from those of 6H-SiC polytype as shown in the above calculated X-ray diffraction, but then, the Raman spectroscopy which is differently classified by the SiC polytypes, can become a strong means to distinguish the SiC polytypes. The outstanding differences between the 3C-SiC and the 6H-SiC were observed at TO and LO regions. In the TO region, the 6H-SiC (799 $cm^{-1}$)· shows a weak peak at the nearly same position as the 3C-SiC (797 $cm^{-1}$). This weak peak of the 6H-SiC to the original mode of the TO phonon branch in the large zone with $E_1$ symmetry. Figure 7 (a) shows the Raman spectrum of the SiC epilayer. TO phonon peaks were observed at 768 $cm^{-1}$, 790 $cm^{-1}$ and 799 $cm^{-1}$, while, LO phonon peak at 967 $cm^{-1}$. It was kno-wn that the allowed modes for Raman scattering in backscattering are $A_1$

and $E_2$ modes [9]. In the LO region, the peak position of the 6H-SiC is different from that of the 3C-SiC. Consequently, the 6H-SiC epilayer has been identified by using the X-ray diffraction and assisting the Raman spectroscopy.

## 5. Conclusions

A SiC epilayer on the 6H-SiC crystal substrate was grown by CVD. The crystal structure of the SiC epilayer was investigated by using the X-ray diffraction patterns and the Raman scattering spectroscopy. It was identified that the SiC epilayer on the 6H-SiC substrate was grown to be homoepilayer by CVD. The 6H-SiC crystal substrates were identified by the five weak sub-peaks of the diffraction pattern. Then, they are rotated constantly along the c-axis during the measurement of the X-ray diffraction.

In order to distinguish a certain SiC polytype mixed in the SiC crystal grown by modified Lely method, we have calculated the X-ray diffraction intensities and Bragg angles of the typical SiC crystal powders. By comparing the measured X-ray diffraction lines with the calculated ones, it was identified that the SiC crystal grown by modified Lely method was the 6H-SiC crystal mixed some 15R-SiC.

## Acknowledgment

The authors are very grateful to professor H. Matsunami and Dr. T. Kimoto at Kyoto University in Japan for their helping to grow the SiC epilayer by CVD.

## References

[1] W.S. Yoo, Polytype Control in Crystal Growth of SiC for Semiconductor Devices (Thesis of Doctor Degree, Kyoto Univ., 1991) p.9.

[2] D.W. Feldman, J.H. Parker, W.J. Choyke and L. Patrick, Phys. Rev. 170 (1968) 698.

[3] S. Nakashima, H. Katahama, Y. Nakakura and A. Mitsuishi, Phys. Rev. B 33 (1986) 5721.

[4] H. Okumura, E. Sakuma, J.H. Lee, H. Mukaida, S. Misawa, K. Endo and S. Yoshida, J. Appl. Phys. 61(3) (1987) 1134.

[5] T. Kimoto, Step-Controlled Epitaxial Growth of $\alpha$-SiC and Device Applications (Thesis of Doctor Degree, Kyoto Univ., (1995) pp.19-88.

[6] M. Kanaya, J. Takahashi, Y. Fujiwara and A. Moritani, Appl. Phys. Lett. 58(1) (1991) 56.

[7] B.D. Cullity, Elements of X-ray Diffraction, Addison-Wesley Pub. Co. INC, 2nd Ed., (Massachusetts, 1978) p.126.

[8] K.S. Park, K.A. Lee, H.B. Lee and Y.B. Kim, 물리교육 13(1) (1995) 42.